Structural Analysis of Synthetic Peptide Fragments from EmrE, a Multidrug Resistance Protein, in a Membrane-Mimetic Environment†

Janani Venkatraman, G. A. Nagana Gowda, and Padmanabhan Balaram*

Molecular Biophysics Unit and Sophisticated Instruments Facility, Indian Institute of Science, Bangalore 560 012, India

ABSTRACT: EmrE, a multidrug resistance protein from *Escherichia coli*, renders the bacterium resistant to a variety of cytotoxic drugs by active translocation out of the cell. The 110-residue sequence of EmrE limits the number of structural possibilities that can be envisioned for this membrane protein. Four helix bundle models have been considered [Yerushalmi, H., Lebendiker, M., and Schuldiner, S. (1996) *J. Biol. Chem. 271*, 31044−31048]. The validity of EmrE structural models has been probed experimentally by investigations on overlapping peptides (ranging in length from 19 to 27 residues), derived from the sequence of EmrE. The choice of peptides was made to provide sequences of two complete, predicted transmembrane helices (peptides **H1** and **H3**) and two helix−loop−helix motifs (peptides **A** and **B**). Peptide (**B**) also corresponds to a putative hairpin in a speculative β-barrel model, with the "Pro-Thr-Gly" segment forming a turn. Structure determination in SDS micelles using NMR indicates peptide **H1** to be predominantly helical, with helix boundaries in the micellar environment corroborating predicted helical limits. Peptide **A** adopts a helix−loop−helix structure in SDS micelles, and peptide **B** was also largely helical in micellar environments. An analogue peptide, **C**, in which the central "Pro-Thr-Gly" was replaced by "^{D}Pro-Gly" displays local turn conformation at the ^{D}Pro-Gly segment, but neither a continuous helical stretch nor β-hairpin formation was observed. This study implies that the constraints of membrane and micellar environments largely direct the structure of transmembrane peptides and proteins and study of judiciously selected peptide fragments can prove useful in the structural elucidation of membrane proteins.

Multidrug resistance pumps (MDRs)[1] are membrane translocases that have the ability to extrude a variety of unrelated cytotoxic drugs from the cell (*1*−*4*). MDRs are present in a wide range of organisms and are mostly very large proteins ranging between 400 and 1500 amino acids in length (*1*), for example, the ABC (ATP binding cassette) transporters (*5*−*7*), and the TEXAN family of bacterial and fungal antiporters (*3*, *4*, *8*). There also exists a family of MDRs represented by very small proteins (100−120 amino acids), which perform functions analogous to their larger cousins (*9*−*10*). This unique family, called Smr (small multidrug resistance proteins) or mini-TEXANs, renders bacteria resistant to a wide variety of toxic, lipophilic cations and has three main members: EmrE from *Escherichia coli* (*11*−*13*), Smr (*14*−*16*), and QacE (*17*) from *Staphylococcus aureus*.

The clinical relevance of the MDR proteins makes their structure elucidation important and desirable. However, their large size limits the application of traditional structure determination techniques. The availability of the mini-TEXANs, which are small, yet possess similar function, makes them ideal model systems to base studies on multidrug resistance. Of all the mini-TEXANs, EmrE is the best studied to date (*18*). EmrE also has the unique property of being not only soluble in mixtures of organic solvents, such as chloroform and methanol, but also functionally active when reconstituted from such solvents (*13*, *19*).

Atomic resolution structures of membrane proteins are scarce. There exist only 33 unique examples of membrane protein crystal structures in the PDB, of which 21 possess a helical bundle topology and 12 are β-barrels (webpage of Stephen White, University of California at Irvine, as of 25 August 2001. URL: http://blanco.biomol.uci.edu/Membrane_Proteins_xtal.edu). Alternate techniques of exploring structure such as NMR (*20*−*21*) and cryo-electron microscopy (*22*−*23*) have seen some success, but have not resulted in very many more examples. Topological clues obtained from sequence analysis, mutagenesis, labeling experiments, and spectroscopic techniques such as FTIR or circular dichroism have often been used as the basis for the construction of three-dimensional models (*24*−*32*). Structural information on membrane proteins has also been derived from the study of synthetic peptide fragments (*33*−*40*) in a variety of membrane mimicking solvents such as chloroform and trifluoroethanol (TFE) (*41*−*43*), in detergent micelles (*43*−*45*), and in lipid vesicles and bilayers (*45*−*48*).

Here we describe attempts at the structure elucidation of EmrE. This study was originally intended to consider two alternate structural models for the protein, a helical bundle

† This work was supported by the Department of Biotechnology under program support for the area "Drug and Molecular Design".

* To whom correspondence should be addressed: Molecular Biophysics Unit, Indian Institute of Science, Bangalore 560 012, India. Fax: +91-80-3600683, +91-80-3600535; Tel: +91-80-3602741; E-mail: pb@mbu.iisc.ernet.in.

[1] Abbreviations: MDR, multidrug resistance pump; NMR, nuclear magnetic resonance; PDB, protein data bank; MALDI-MS, matrix-assisted laser desorption ionization mass spectrometry; NOE, nuclear Overhauser effect; TFA, trifluoroacetic acid; TFE, trifluoroethanol; SDS, sodium dodecyl sulfate; TSP, trimethylsilylpropionate; RMSD, root-mean-square deviation; TMS, transmembrane segment; EDT, ethanedithiol; DCM, dichloromethane.

10.1021/bi015793w CCC: $22.00
Published on Web 05/01/2002

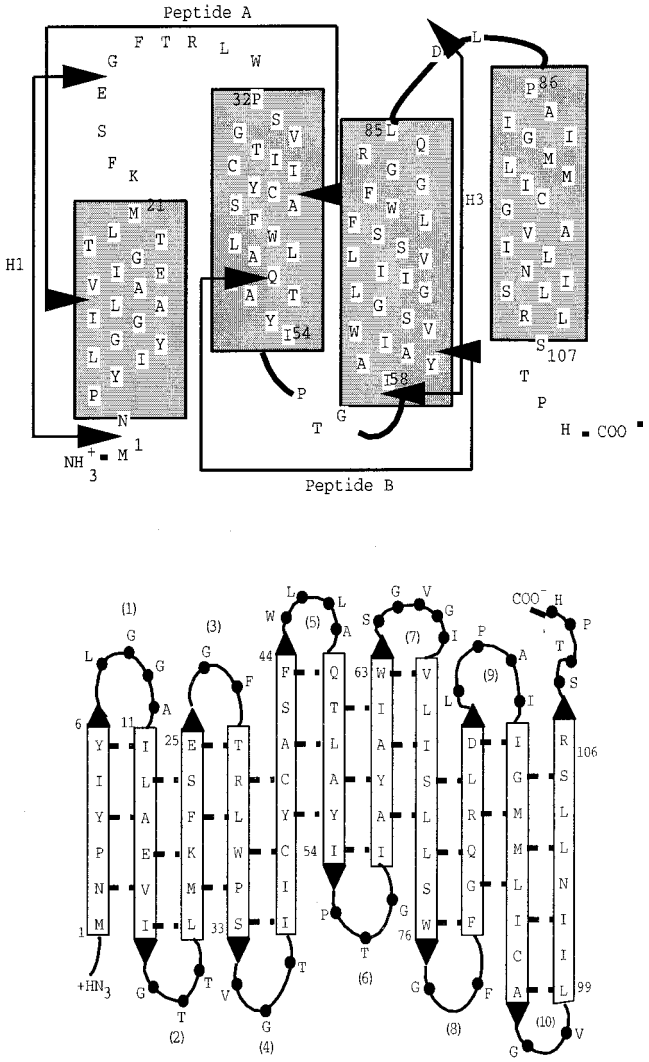

FIGURE 1: (Top) Schematic representation of the helical bundle model for EmrE (*19*, *49*) with the location of synthetic peptides marked on the protein sequence by arrows. (Bottom) The division of the EmrE sequence into 11 strands connected by 10 tight turns. The constituent hairpins are labeled 1−10.

model and a β-barrel model, whose validity could be experimentally ratified by the study of synthetic peptides chosen from appropriate regions of the protein. EmrE has been popularly modeled as a four helix bundle (Figure 1, top) in the literature (*20*, *49*), and recent structural investigations on the protein by other groups provide some support for a predominantly helical structure (*50*−*51*), which functions as an oligomer (*19*). Also, construction of a stereochemically acceptable 11-stranded β-barrel model itself revealed that the resultant barrel height is insufficient to traverse the membrane bilayer without resulting in energetically unfavorable effects such as membrane dimpling (*52*−*53*).

It is pertinent to note that the structural investigations thus far performed, FTIR (*50*), multidimensional NMR in mixtures of organic solvents (*51*), and cryo-electron microscopy (*54*), have failed to provide a three-dimensional model for the protein. In the absence of such a structure, we present studies on overlapping, synthetic peptide fragments derived from the sequence of EmrE. The choice of peptides was made to provide sequences of two complete, predicted transmembrane helices [the transmembrane segments (TMS) 1 and 3: peptides **H1** and **H3**] and two helix−turn−helix motifs (TMS1−loop−TMS2, peptide **A** and TMS2−turn−TMS3, peptide **B**) (Figure 1, top). One such helix−turn−helix peptide (**B**) also happened to correspond to hairpin 6 in the β-barrel model (Figure 1, bottom). Peptide **B** contains a "PTG" motif predicted to form the turn segment. An analogue peptide, **C**, in which PTG was replaced by "^{D}PG", was also synthesized. "^{D}Pro-Xxx" motifs have often been utilized for the nucleation of β-hairpin structures as they form tight type I′ or II′ β-turns (*55*−*56*). Peptide **C** could act as a control peptide to assay any incipient beta structure in peptide **B**. Additional "GR" segments were appended to the N- and C-termini of peptides **B** and **C** to enhance solubility and discourage lateral aggregation in the event of β-hairpin formation. In peptide **A**, the penultimate Ile residue present in the original protein sequence was mutated to a Trp residue to provide a fluorophore that can be potentially positioned at a membrane interface. The existing Trp residue in the sequence was hence replaced conservatively by Phe. The protein sequence corresponding to peptide **H3** contains two Trp residues (Figure 1); Trp(76) (EmrE numbering) was changed to an Ile residue in the synthesized peptide **H3** to ensure the presence of a unique fluorophore. The following sequences were synthesized and characterized:

H1 (24 residues): Ac-NPYIYLGGAILAEVIGTTLMKFSE-NH_2

H3 (27 residues): IAYAIWSGVGIVLISLLSIGFFGQRLD-NH_2

A (24 residues): VIGTTLMKFSEGFTRLFPSVGTWI-NH_2

B (19 residues): RGQYLAYIPTGIAYAIWGR-COOH

C (18 residues): RGQYLAYI^{D}PGIAYAIWGR-COOH

Peptide **H1** was acetylated at the N-terminus, and peptides **H1**, **H3**, and **A** were amidated at the C-terminus.

High-resolution NMR experiments, performed in membrane-mimetic environments such as SDS micelles, have permitted structural analysis of peptides **H1**, **A**, **B**, and **C**. The studies described here establish that the synthetic peptides are predominantly helical in nature, with experimentally derived helix boundaries agreeing with predicted helix limits in the helical bundle model. The ^{D}Pro-Gly motif is unsuccessful in nucleating β-hairpin conformations in peptide **C** in a membrane-mimetic environment, although formation of a local β-turn is observed.

MATERIALS AND METHODS

Materials. Chemicals used in solid-phase synthetic procedures were obtained from Novabiochem (Nottingham, UK), Bachem (Bubendorf, Switzerland), or Sigma (St. Louis, MO). Trifluoroacetic acid (TFA) and piperidine were purchased from Chem-Impex International Inc. (Wood Dale, IL), and the resins used in peptide synthesis (PAL-PEG-PS and PR500) from PerSeptive Biosystems (Hertford, UK) and Novabiochem (Nottingham, UK), respectively. Sodium dodecyl-d_{25} sulfate utilized in NMR experiments was purchased from Cambridge Isotope Laboratories (Andover, MA). All other chemicals used were from local manufacturers such as Ranbaxy and E. Merck, India.

Peptide Synthesis and Purification. Peptides **H1**, **H3**, **A**, **B**, and **C** were synthesized on a LKB-Biolynx 4175

semiautomatic peptide synthesizer using standard Fmoc (9-fluorenylmethyloxycarbonyl) chemistry. Peptides **B** and **C** were assembled on PAC-PEG-PS resin, and peptides **H1**, **H3**, and **A** were synthesized on a Fmoc derivatized polydimethyl acrylamide resin, PR500. Following complete synthesis, the N-terminus of **H1** was acetylated by standing in an equimolar mixture of acetic anhydride/acetic acid for 5 h. Peptides **B** and **C** were simultaneously cleaved off the resin and deprotected using a cleavage cocktail containing trifluoroacetic acid (TFA), 5% anisole, and 1% ethane dithiol (EDT). Peptides **H1**, **H3**, and **A** were cleaved off the resin and deprotected in two successive steps: cleavage was achieved by treating the resin with a solution of 10% TFA in dichloromethane (DCM) for 1.5 h. The resin was then filtered off, the TFA/DCM mixture was evaporated in vacuo, and a deprotection cocktail of 94% TFA, 5% anisole and 1% EDT was added. Peptides assembled on the PR500 resin (**H1**, **H3**, and **A**) were obtained as their acid amides, while peptides **B** and **C** are free acids. Following complete deprotection, the peptides were precipitated using ether and purified by reverse-phase high performance liquid chromatography (HPLC) on a C_{18} column ($5-10\mu$, 7.8×250 mm) using water/acetonitrile/TFA gradients. The purified peptides were characterized using matrix-assisted laser desorption ionization mass spectrometry (MALDI-MS) on a Kratos Analytical (UK) Kompact Seq model, which uses a 337 nm nitrogen laser for laser desorption and 1.7 nm linear flight path. The instrument was calibrated over the low mass range of 300−5000 Da using standard samples of known molecular weights. [**H1**: $M_{calc} = 2643.1$, $M_{obs} = 2642.6$ (MH^+), 2664.1 ($M + Na^+$), 2683.4 ($M + K^+$); **A**: $M_{calc} = 2688.1$, $M_{obs} = 2689.6$ (MH^+); **B**: $M_{calc} = 2107.4$, $M_{obs} = 2108$ (MH^+), 2130.6 ($M + Na^+$), 2146.1 ($M + K^+$); **C**: $M_{calc} = 2006.3$, $M_{obs} = 2007.1$ (MH^+)].

Circular Dichroism. Circular dichroism spectra were recorded on a JASCO J-715 CD spectropolarimeter. Spectra were recorded between 250 and 195 nm (0.1 cm cell, peptide concentration ~100 μM) at 0.1-nm intervals with a time constant of 4 s at 313 K and a scan speed of 20 nm/min and averaged over four separate scans. The spectra obtained were baseline corrected and smoothed. Peptide concentrations were determined using the molar extinction coefficient of Tyr (~1420 M^{-1} cm^{-1})/Trp (~5600 cm^{-1}).

NMR Spectroscopy. ^{1}H NMR experiments were carried out on a Bruker DRX500 spectrometer. One-dimensional experiments were acquired using 32K data points and processed with 1 Hz line broadening. 2D experiments were performed in the phase sensitive mode with time proportional phase incrementation. The sodium salt of trimethylsilylpropionate (TSP) in water was used to reference chemical shifts. Peptides, at a concentration of 1 mM in 10%D_2O/90%H_2O (pH ~ 3.0) containing 100 equiv of SDS, were subjected to TOCSY (*57*), NOESY (*58*), and DQF−COSY (*59*) experiments at 313 K. Mixing times of 104 and 300 ms, respectively, were used for TOCSY and NOESY experiments. All 2D experiments were performed by collecting 2 K data points in f2 and 512 data points in f1 using a spectral width of 6009.6 Hz. Solvent suppression was achieved using watergate sequences with standard pulse sequences available in the Bruker library. NMR data were processed using Bruker XWINNMR software on a Silicon Graphics Indy workstation. A shifted (π/2) sine-squared window function was applied prior to Fourier transform in both the dimensions and zero-filling to 2K points was applied to data in f1.

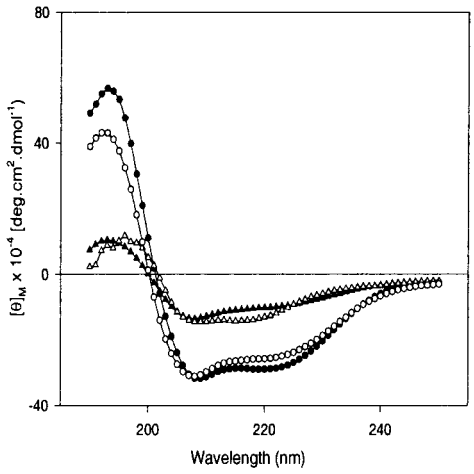

FIGURE 2: CD spectra of peptides **H1** (●), **A** (○), **B** (Δ), and **C** (▲) in 10 mM SDS (313 K).

Structure Calculation. NOEs obtained from NOESY spectra were visually classified as strong, medium, and weak and used to derive upper and lower distance constraints [strong: 2.0−2.5 Å, medium 2.5−3.5 Å, weak: 3.5−4.5 Å). Hydrogen exchange experiments for the purpose of obtaining information about hydrogen bonded residue pairs were not performed as amide protons are protected from H/D exchange by both peptide structure and the SDS micelle, and it is difficult to distinguish between their relative effects. Hence, hydrogen bonding constraints were not used in structure calculations. A total of 218, 216, and 172 distance constraints were applied to structure calculations performed for peptides **H1**, **A**, and **B**, respectively, using DYANA 1.5 (*60*). Ten structures with the lowest energy, showing least violation of constraints, were picked out, and a superposition was calculated using MOLMOL (*61*).

RESULTS

EmrE-derived peptides demonstrated poor solubility in water and a range of organic solvents following lyophilization. Indeed, purification of peptide **H3** was not possible as the peptide was insoluble in water and all organic solvents compatible with HPLC, and was hence not studied further. However, peptides **H1**, **A**, **B**, and **C** were soluble in fluoro alcohols (such as trifluoroethanol (TFE)) and detergent solutions (such as SDS). They were hence studied in SDS micelles at a peptide/SDS ratio of 1:100. This ratio was chosen to ensure that a single peptide molecule was present per micelle; the aggregation number of SDS is close to 70 (*62*). In all studies, the concentration of SDS was above its critical micellar concentration (~7 mM).

Molecular Structure of H1. The far UV CD spectrum of **H1** in SDS micelles (Figure 2) is indicative of a classical helical pattern (*63*) with spectral minima at 222 and 208 nm. The CD bands are characterized by high intensity and hence suggestive of a large population of structured molecules. The helical CD pattern is consistent with the observation of many amide and C^α proton resonances at high field positions in the one-dimensional ^{1}H NMR spectrum of **H1** (data not shown). The line-widths in the 1D spectrum of **H1** in SDS micelles are rather broad, a feature consistent with the fact

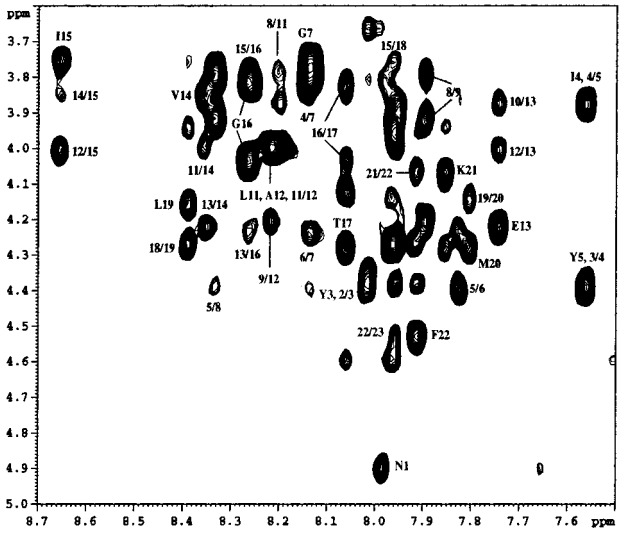

FIGURE 3: Partial expansion of the NOESY spectrum of **H1** with many key $C^{\alpha}H/NH$ NOEs highlighted.

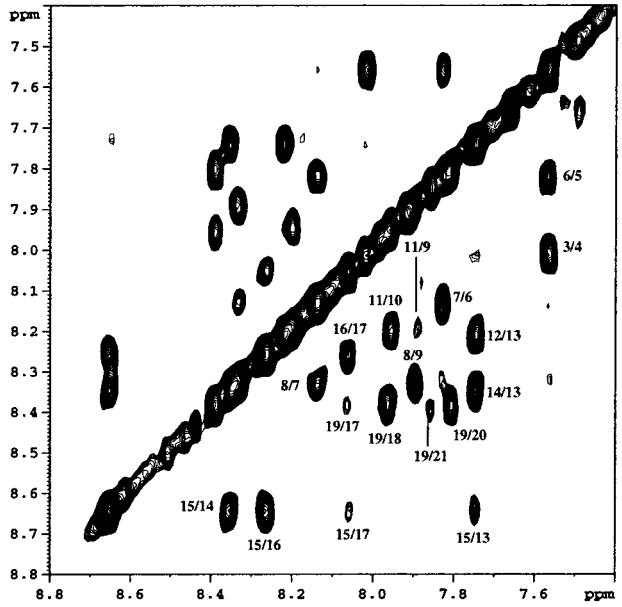

FIGURE 4: Portion of the NOESY spectrum of **H1** illustrating a continuous stretch of $NH/N_{i+1}H$ NOEs from residues 3−20.

that the system under observation corresponds to a mass far exceeding that of the free peptide. The average SDS micelle is expected to be comprised of over 60−70 detergent molecules (*62*), resulting in a large complex, slower tumbling rates and hence broad lines. However, the spectrum is well dispersed with little overlap, enabling complete NMR analysis of the peptide. A combination of TOCSY, NOESY, and DQF−COSY experiments were utilized to obtain sequence-specific assignments for all experimentally observed protons.

Spectra obtained from NOESY experiments revealed various features consistent with helical structure, such as significantly more intense intraresidue $C_i^{\alpha}H/N_iH$ NOEs as compared to the corresponding interresidue $C^{\alpha}H/N_{i+1}H$ NOE (Figure 3). In addition, a continuous stretch of sequential NH/NH NOEs (Figure 4), from residues 3−20 [Tyr(3)−Met-(20)] were observed, as well as many $N_iH/N_{i+2}H$ NOEs [A9/L11, E13/I15, I15/T17, T17/L19 AND L19/K21], strongly indicating local helical [α_R] conformations at these residues.

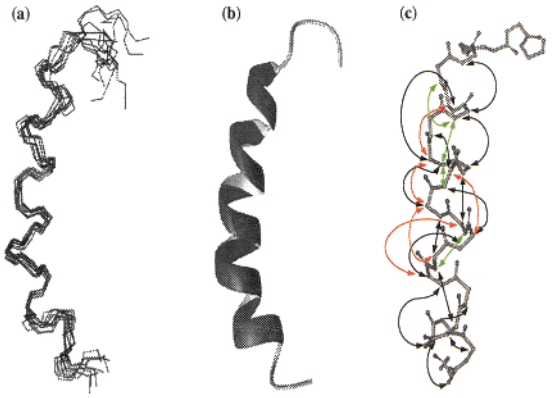

FIGURE 5: (a) Superposition of 10 best structures calculated from NMR-derived distance constraints. (b) Ribbon representation of the mean structure of **H1**. Note the continuous helix from residues 2−20. (c) Ball and stick model of the mean structure of **H1** with observed long-range NOEs marked [black: $C^{\alpha}_iH/N_{i+3}H$ NOEs, green: $N_iH/N_{i+2}H$ NOEs]. C^{β} atoms are not explicitly illustrated in panel c; red arrows between two backbone C^{α} atoms represent $C^{\alpha}_iH/C^{\beta}_{i+3}H$ NOEs.

The establishment of long-range order is necessarily accompanied by interactions between residues that are not adjacent in sequence. In helical structures, residues separated by a single turn of the helix are brought into close structural proximity, resulting in interactions involving both backbone and backbone and side chain atoms. Indeed, many $C_i^{\alpha}H/C_{i+3}^{\beta}H$ NOEs [G8/L11, A9/A12, I10/E13, A12/I15, I15/T18] and an almost continuous stretch of $C_i^{\alpha}H/N_{i+3}H$ NOEs [P2/Y5, Y3/L6, I4/G7, Y5/G8, L6/A9, G7/I10, G8/L11, A9/A12, I10/E13, A12/I15, E13/G16, V14/T17, I15/T18, T17/M20, T18/K21] are observed (Figures 3 and 5c), establishing the presence of a substantial stretch of helix in **H1**.

The sequence of peptide **H1** has a proline residue at the position 2. Strong $C^{\alpha}H$(Asn(1))−$C^{\delta}H$(Pro(2)) NOEs indicate the Asn−Pro bond to be in the trans conformation. The observation of a medium intensity Pro(2)−Tyr(5) $C^{\alpha}H/N_{i+3}H$ NOE is supportive of the inclusion of Pro(2) in the peptide helix.

The 109 observed NOEs were translated into distance constraints for structure calculations, and DYANA (*60*) was employed to obtain an ensemble of NMR-derived structures for **H1**. Figure 5a displays the superposition [RMSD 0.84 (± 0.25) Å] of 10 best structures calculated using DYANA, and Figure 5b illustrates the mean structure obtained from the superposition.

The low value of RMSD is a reflection of the extensive network of NOEs defining proton−proton interactions in the sequence of **H1**. **H1** is a continuous helix from residues 2−20, with helical conformation initiating at Pro(2). The $N-C^{\alpha}$ torsion angle, ϕ, of the ^{L}Pro residue is restricted to −60° (± 20°), and as a consequence, the local conformations of ^{L}Pro are largely limited to $\psi \sim -30°$ (± 20°) [α_R] or $\psi \sim +120°$ (± 30°) [polyproline conformation]. ^{L}Pro, in the $\phi = -60°$ (± 20°), $\psi = +120°$ (± 20°) conformation results in helix termination (64). However, ^{L}Pro, in the $\phi = -60°$ (± 20°), $\psi = -30°$ (± 20°) conformation, is compatible with helical structure, and hence, it is not surprising that **H1** forms an extended helix ranging from residues Pro(2)−Met-(20).

The experimentally obtained helix limits of **H1** (Figure 5) correlate remarkably well with the predicted helix

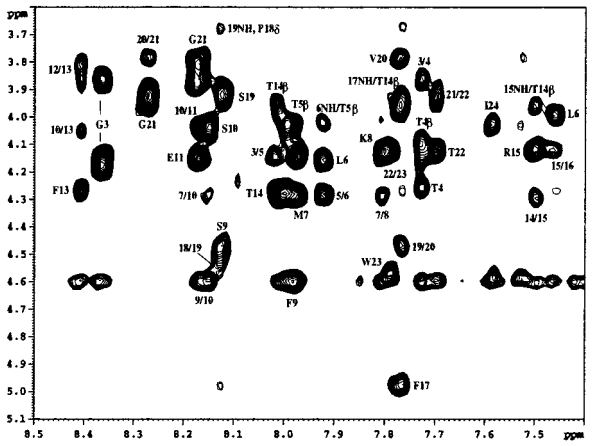

FIGURE 6: Partial expansion of the NOESY spectrum of **A** with several key $C^{\alpha}H/N_{i+3}H$ NOEs marked.

boundaries of TMS1 in EmrE (Figure 1, top). While the hydrophobic stretch comprising residues 2−20 of peptide **H1** is expected to insert into the micelle core and, as a consequence, adopt helical conformation, such an observation, nevertheless, corroborates the application of membrane-mimetic environments such as detergents to the study of transmembrane peptides and proteins.

Solution Conformation of Peptide A. The sequence of peptide **A** corresponds to the upper half of TMS1, the long loop succeeding it, and the upper half of TMS2 (Figure 1), forming a potential helix−loop−helix motif. This is reflected in the far-UV CD of **A**, which is very similar to that of **H1** (Figure 2), and displays an intense helical signature.

High-resolution NMR techniques were applied to the structure determination of peptide **A** in SDS micelles. Sequence-specific residue assignments were obtained from TOCSY, NOESY, and DQF−COSY experiments. As in the case of **H1**, the NOESY spectrum of **A** reveals strong $C_i^{\alpha}H/N_iH$, weaker $C_i^{\alpha}H/N_{i+1}H$ (Figure 6), and many strong $NH/N_{i+1}H$ NOEs [G3/T4, T4/T5, L6/M7, M7/K8, K8/F9, F9/S10, G12/F13, F13/T14, T14/R15, R15/L16, L16/F17, S19/V20, V20/G21, G21/T22, T22/W23, W23/I24] (Figure 7), signifying the presence of local helical conformations. Observation of many $C_i^{\alpha}H/N_{i+3}H$ [G3/L6, T4/M7, T5/K8, L6/F9, M7/S10, S10/F13, E11/T14, F13/L16, T14/F17, L16/S19, F17/V20, P18/G21, S19/T22, V20/W23, G21/I24] and $C_i^{\alpha}H/C_{i+3}^{\beta}H$ [T4/M7, T5/K8, L6/F9, M7/S10, S10/F13, G12/R15, F13/L16, T14/F17, R15/P18, L16/S19, F17/V20, V20/W23] NOEs throughout the peptide sequence further attests to peptide **A** possessing a long stretch of helix (Figure 8c).

The sequence of peptide **A** contains a Pro residue at position 18. Strong Trp(17)$C^{\alpha}H$/Pro(18)$C^{\delta}H$ NOEs confirm that the Trp−Pro bond is in the trans conformation. The observation of long range, weak Arg(15)/Pro(18) $C_i^{\alpha}H/C_{i+3}^{\beta}H$ and Pro(18)/Gly(21) $C_i^{\alpha}H/N_{i+3}H$ NOEs establish that the proline residue is accommodated in the helix. The incorporation of Pro into transmembrane helices is widespread and has previously been observed in many integral membrane proteins (*65*).

A combination of $NH/N_{i+1}H$, $C_i^{\alpha}H/N_{i+3}H$, and $C_i^{\alpha}H/C_{i+3}^{\beta}H$ NOEs are essential to accurately determine the perpetuation of helicity along the entire peptide sequence. Scrutiny of the NOESY spectrum of **A** disclosed the absence of several key NH/NH [S10/E11, E11/G12], $C_i^{\alpha}H/N_{i+3}H$ [K8/E11, F9/G12, G12/R15], and $C_i^{\alpha}H/C_{i+3}^{\beta}H$ [K8/E11, F9/G12] NOEs (Figure 8c), implying residues 8−12 to be less structured than the rest of the peptide.

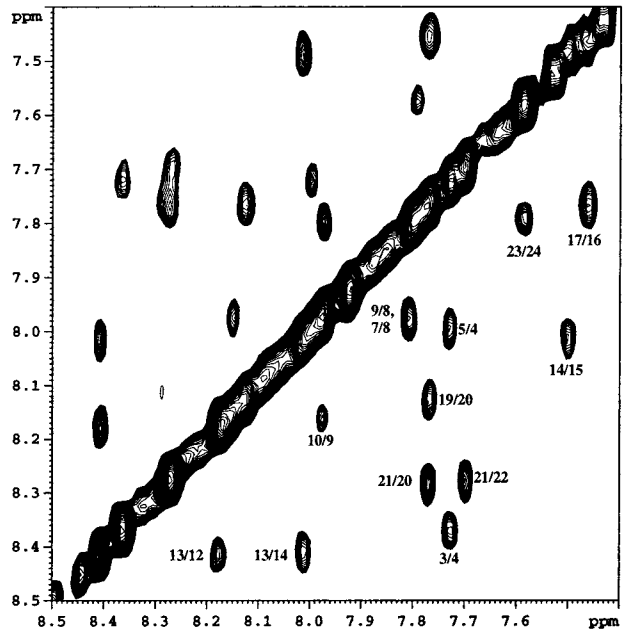

FIGURE 7: Portion of the NOESY spectrum of **A** illustrating the presence of $NH/N_{i+1}H$ NOEs.

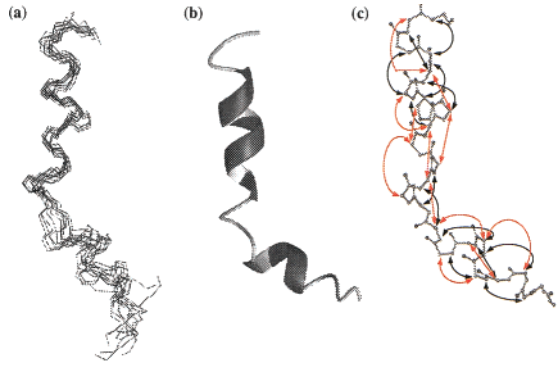

FIGURE 8: (a) Superposition of 10 best structures obtained from structure calculations using DYANA (*60*). (b) Ribbon representation of the mean structure for **A**. Note the presence of two distinct helical segments interspersed by an unstructured region. (c) Backbone of peptide **A** with observed NOEs marked [black: $C_i^{\alpha}H/N_{i+3}H$ NOEs, red: $C_i^{\alpha}H/C_{i+3}^{\beta}H$ NOEs]. Again, C^{β} atoms are not explicitly illustrated in panel c.

Figure 8c is a schematic representation of observed NOEs; note the clustering of long-range NOEs in N- and C-terminal segments of **A** with a less well-defined internal stretch. This is reflected in the collection of structures calculated for **A** using DYANA (*60*): Figure 8a (a superposition of 10 best structures, RMSD 1.31 (± 0.59) Å for residues 13−22) and Figure 8b display two distinct helical segments (residues 3−7 and 13−22) separated by a less structured region (residues 8−12)—a helix−loop−helix motif. It is pertinent to note that the extreme residue redundancy in the sequence of EmrE, and hence the synthetic peptides, precludes the reliable assignment of long-range side chain−side chain NOEs involving residues in the N- and C-terminal helical segments. In the absence of such defining interactions, the structure of peptide **A** does not converge into a helical hairpin as desired in the context of the protein structure and must merely be characterized as a helix−loop−helix motif.

Comparison of the experimentally derived structures of peptides **H1** and **A** with the predicted helices of EmrE indicate many interesting correlations. The sequence motif -VIGTTLMKFSE- is common to peptides **H1** and **A**, and strikingly, this sequence adopts similar conformations in both synthetic peptides: the -GTTLM- segment is helical, while -KFSE- is unstructured in both cases. While the above structural demarcations are perhaps not entirely unexpected in the case of **H1**, the observation of a centrally located unstructured region connecting two helical segments augurs well for the application of synthetic peptide studies for the deduction of protein structure and suggests that, as predicted, TMS1 terminates at residue M(21) [protein numbering] (Figure 1, top). However, the C-terminal helical segment of **A** (residues 13−22) (peptide **A** numbering, Figure 8) does not agree with the boundaries of TMS2 as predicted in the helical bundle model (Figure 5.1, top); the peptide helix extends N-terminally to four more residues than predicted for TMS2. This could be because the positively charged Arg(15) residue interacts favorably with the negatively charged surface of the micelle, inducing local helical conformation and extending the peptide helix to Phe(13). However, a longer transmembrane segment 2 is hardly incompatible with the four helix bundle model and merely requires this segment to be tilted at a greater angle to the membrane normal to accommodate more residues in the hydrophobic bilayer and to permit the arginine residue (Arg(29), EmrE numbering) to interact with the negatively charged head of the phospholipid groups. In the absence of experiments such as the effect of micelle-incorporated spin labels on signal broadening, which directly assay the positioning of various residues in the detergent micelle (in the hydrophobic core, at the surface or in bulk solvent) (*66*−*67*), such an interpretation must merely remain a hypothesis.

NMR Determined Structures of Peptides B and C in SDS Micelles. The sequence of synthetic peptide **B** [RGQYLAY-IPTGIAYAIWGR] is designed to correspond to the lower portion of TMS2, the tight PTG turn, and the lower portion of TMS3 in the four helix bundle model, and to putative hairpin 6 in the β-barrel model. Peptide **C** [RGQYLAYI^{D}-PGIAYAIWGR], which differs from **B** only in the turn segment (the PTG motif has been substituted with ^{D}PG), can serve as a control peptide in structure determination studies. Analysis of the CD spectra of **B** and **C** indicates peptide **B** to be in helical conformation, although with greatly reduced signal intensities as compared to peptides **H1** and **A** (Figure 2). The CD signature of **C** is very similar to that of **B**, although careful inspection reveals contributions from an additional band between 215 and 220 nm (Figure 2), suggesting the presence of β-turn conformations.

NMR analysis (Figures 9 and 10) of **B** again resulted in the observation of many NOEs consistent with helical structure [intense $C_i^{\alpha}H/N_iH$, weak $C_i^{\alpha}H/N_{i+1}H$, and many continuous $NH/N_{i+1}H$ NOEs]. Medium and weak intensity $C_i^{\alpha}H/N_{i+3}H$ and $C_i^{\alpha}H/C_{i+3}^{\beta}H$ NOEs (Figure 11c) confirm the helical nature of peptide **B**. Structure calculations resulted in an ensemble of structures for peptide **B** (Figure 11), with residues Ile(8)−Ile(16) forming a continuous helix (RMSD 0.79 (± 0.22) Å). Pro(9) is again accommodated in the helical segment, as evinced by the observation of a weak Pro(9)/Ile(12) $C_i^{\alpha}H/N_{i+3}H$ NOE.

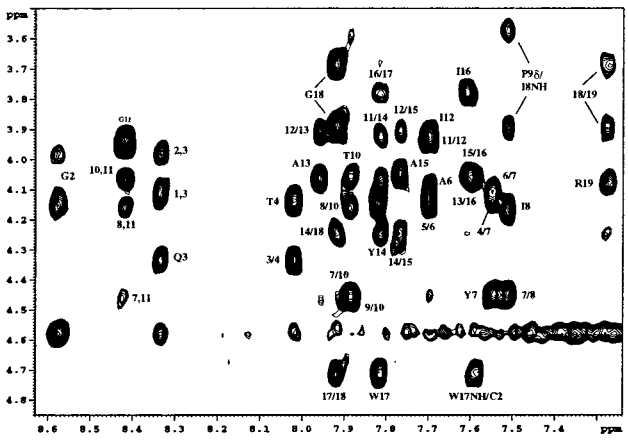

FIGURE 9: Portion of the NOESY spectrum of **B** illustrating the various $C^{\alpha}H/NH$ correlations observed.

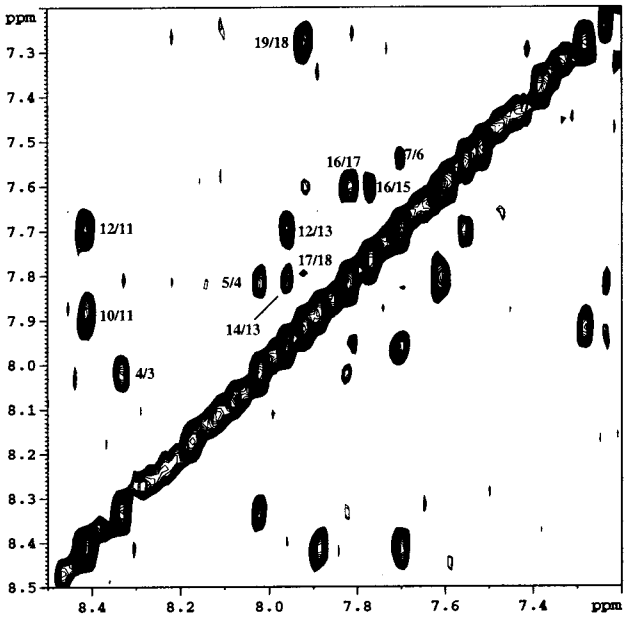

FIGURE 10: Portion of the NOESY spectrum of **B** illustrating the presence of sequential NH/NH NOEs.

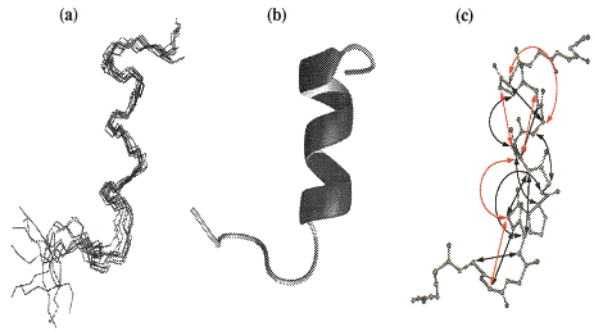

FIGURE 11: (a) Superposition of 10 best structures of peptide **B** calculated using DYANA (*60*). (b) Structure of peptide **B**. (c) Schematic diagram of the peptide backbone with observed NOEs marked [black: $C_i^{\alpha}H/N_{i+3}H$ NOEs, red: $C_i^{\alpha}H/C_{i+3}^{\beta}H$ NOEs].

Comparison of the NOESY spectra of peptides **B** and **C** reveals many differences of structural significance: (a) The pattern of strong intraresidue $C_i^{\alpha}H/N_iH$ and weak interresidue $C_i^{\alpha}H/N_{i+1}H$ NOEs observed in the NOESY spectrum of **B** (Figure 9) is absent in peptide **C** (Figure 12). Indeed, the corresponding correlations are of almost equal intensity. (b) The ^{D}Pro(9)−Gly(10) $C_i^{\alpha}H/N_{i+1}H$ (Figure 12) and Gly(10)/

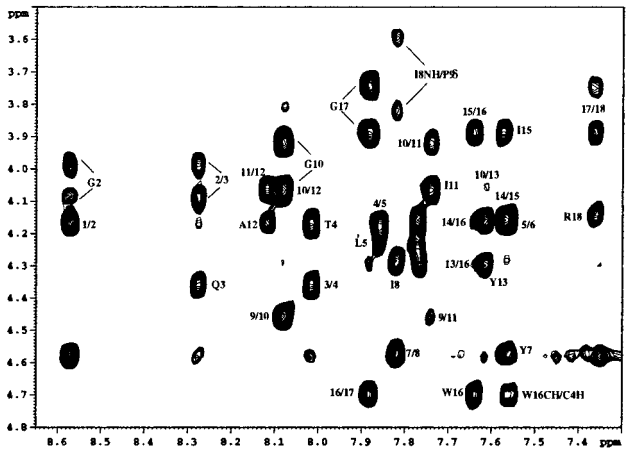

FIGURE 12: Partial expansion of the NOESY spectrum of **C**. Note the absence of long-range $C^{\alpha}H/NH$ NOEs.

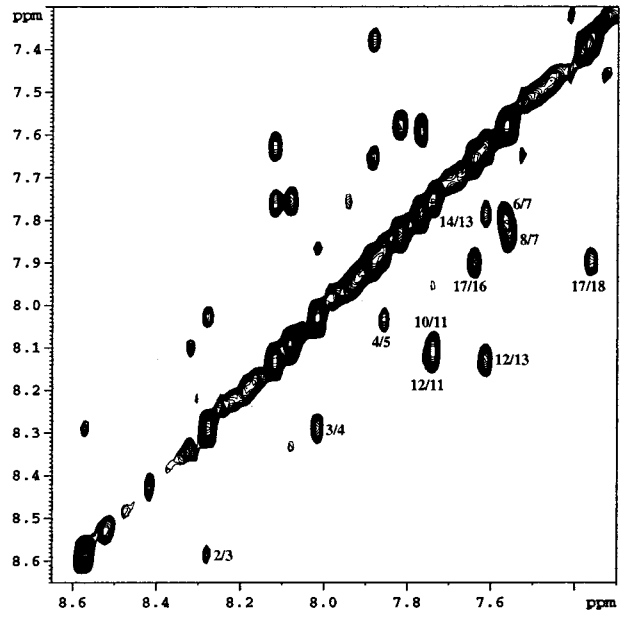

FIGURE 13: NH/NH region of the NOESY spectrum of peptide **C**. Presence of many NH/NH NOEs indicates local helical conformation.

Ile(11) NH/NH correlations in **C** (Figure 13) are significantly intense, suggesting the formation of a type II′ β-turn. The corresponding ^{L}Pro(9)−Thr(10) NOE in **B** (Figure 9) is weak in intensity. (c) The structurally relevant $C_i^{\alpha}H/N_{i+3}H$ and $C_i^{\alpha}H/C_{i+3}^{\beta}H$ NOEs which are a feature of the NOESY spectrum of **B** (Figure 11c) are conspicuously absent in the spectrum of peptide **C**. This suggests that while much local helical conformation is imposed on the residues of **C** due to the hydrophobic core of the detergent micelle (attested to by the many NH/NH NOEs, Figure 13), the ^{D}Pro−Gly motif interrupts the formation of a continuous helix.

Unlike its L-counterpart, the ^{D}Pro residue with its positive value of ϕ cannot be accommodated in the peptide helix. However, in peptide **C**, it has not succeeded in translating the local β-turn conformation into a full fledged β-hairpin, suggesting that the constraints of the micellar environment overwhelmingly dictate the formation of helical structure. Also, correlation of the experimentally observed boundaries for peptide **B** with the predicted structure is not as easily achieved as for peptides **H1** and **A**. Peptide **B** is certainly helical in the SDS micellar environment utilized for structural

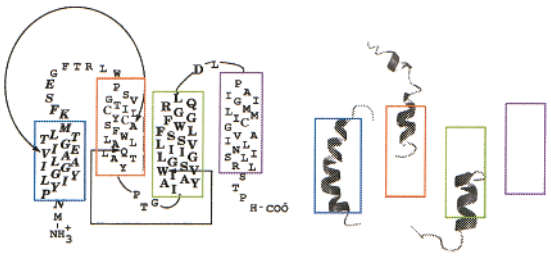

FIGURE 14: The four helix bundle model with predicted helix boundaries of TMS 1, 2, 3, and 4 colored blue, red, green, and violet, respectively. The sequences of synthetic peptides **H1** and **H3** are highlighted as bold residues on the protein sequence, while those of **A** and **B** are demarcated by arrows. Experimentally observed peptide structures are arranged on the right to match the four helix bundle model, with predicted helix limits superposed as colored boxes.

studies, with helical conformation observed between residues 8−16. The desired structure for peptide **B**, as suggested by the four helix bundle model (Figure 1, top), is a helix−turn−helix motif, with helical stretches involving residues Gln(3)−Ile(8) and Ile(12)−Trp(17). The observed structure for peptide **B** incorporates the PTG motif in the single calculated helix. It is possible that the presence of N- and C-terminal arginine residues may prevent the insertion of **B** into the SDS micelle in the desired helix−turn−helix conformation and hinder accurate determination of helix termini.

DISCUSSION

The studies presented here suggest that the structural analysis of synthetic peptide fragments of membrane proteins in membrane-mimetic environments can be utilized to provide information about protein structure. NMR studies of peptides derived from EmrE in membrane-mimetic micellar environments show that peptides **H1**, **A**, and **B** are clearly helical and have resulted in strong indications of helix boundaries. Hence, mapping of the NMR derived structures of the synthetic peptides onto the sequence of EmrE permits the partial reconstruction of protein structure (Figure 14), indicating that the synthesis of the entire EmrE sequence as a series of overlapping peptides might indeed result in a three-dimensional model. Such an approach may, however, be limited by the insoluble nature of chosen fragments. Indeed, in the present study, we were unable to structurally characterize peptide **H3** because of its total insolubility.

Peptide **H1** bears a centrally located glutamic acid residue (Glu(13), **H1** numbering), which has been implicated in the functioning of EmrE (*10*, *68*). Indeed, it is the only charged residue predicted in the entire protein sequence to be present wholly in the hydrophobic core of the membrane (*68*). **H1** forms an extended helical structure from Pro(2)−Met(20) and the highly nonpolar nature of the sequence implies that this stretch traverses the core of the SDS micelle, exposing Glu(13) to the interior of the micelle. However, the accommodation of a charged residue in the membrane interior is energetically unfavorable, and it has been suggested that in the functional EmrE oligomer (*19*) this residue (Glu14, protein numbering) is present in the lumen of the translocase pore.

It is pertinent to note that characterization of secondary structure in membrane-mimetic environments can lead to

uncertain results because of well-documented effects of the lipid on the secondary structure of the peptide (*69*). Understandably, at low, monomeric concentrations of peptides in the bilayer, or even organic solvents, an α-helical conformation in which hydrogen bonding is maximized is more probable than β-strand conformation, which leaves unsatisfied hydrogen bond donors and receptors. This property of the two basic secondary structural elements increases the difficulty, or even precludes, the facile observation of β-strand conformations in small, synthetic transmembrane peptides, even if the conformation of the segment in the native protein were to be extended in nature. However, FTIR and other NMR studies on EmrE (*50*−*51*) unequivocally establish the overwhelming helical content of the protein, indicating that the nonobservation of beta structure is not an artifact of the micellar environment.

While extrapolations from studies of synthetic fragments to intact protein structure always remains suspect, support for such studies can be derived from the observation that expression of pore-lining segments of oligomeric ion channels results in peptide oligomerization and concomitant channel activity (*70*−*72*). The present study relies on this observation to advance structural information for EmrE in the absence of a crystal or NMR structure, and also strongly suggests that the energetic requirements of the micellar and membrane cores may greatly influence the structures of transmembrane proteins and peptides.

SUPPORTING INFORMATION AVAILABLE

^{1}H chemical shifts (from TSP) of peptides **H1**, **A**, **B**, and **C** in 90% H_2O/10% D_2O, 100 mM SDS-d_{25}, pH 3.5, 313 K. This material is available free of charge via the Internet at http://pubs.acs.org.

REFERENCES

1. Lewis, K. (1994) *Trends Biochem. Sci. 19*, 119−123.
2. Marshall, N. J., and Piddock, L. J. (1997) *Microbiologia 13*, 285−300.
3. Nikaido, H. (1998) *Curr. Opin. Microbiol. 1*, 516−523.
4. Van Bambeke, F., Balzi, E., and Tulkens, P. M. (2000) *Biochem. Pharmacol. 60*, 457−470.
5. Doige, C. A., and Ames, G. F. (1993) *Annu. Rev. Microbiol. 47*, 291−319.
6. Schneider, E., and Hunke, S. (1998) *FEMS Microbiol. Rev. 22*, 1−20.
7. van Veen, H. W., and Konings, W. N. (1997) *Semin. Cancer Biol. 8*, 183−191.
8. Nikaido, H. (1994) *Science 264*, 382−388.
9. Paulsen, I. T., Skurray, R. A., Tam, R., Saier, M. H., Jr., Turner, R. J., Weiner, J. H., Goldberg, E. B., and Grinius, L. L. (1996) *Mol. Microbiol. 19*, 1167−1175.
10. Saier, M. H., Jr., Paulsen, I. T., and Matin, A. (1997) *Microb. Drug Resist. 3*, 289−295.
11. Morimyo, M., Hongo, E., Hama-Inaba, H., and Machida, I. (1992) *Nucleic Acids Res. 20*, 3159−3165.
12. Purewal, A. S. (1991) *FEMS Microbiol. Lett. 66*, 229−231.
13. Yerushalmi, H., Lebendiker, M., and Schuldiner, S. (1995) *J. Biol. Chem. 270*, 6856−6863.
14. Littlejohn, T. G., DiBerardino, D., Messerotti, L. J., Spiers, S. J., and Skurray, R. A. (1991) *Gene 101*, 59−66.
15. Littlejohn, T. G., Paulsen, I. T., Gillespie, M. T., Tennent, J. M., Midgley, M., Jones, I. G., Purewal, A. S., and Skurray, R. A. (1992) *FEMS Microbiol. Lett. 74*, 259−265.
16. Grinius, L., Dreguniene, G., Goldberg, E. B., Liao, C. H., and Projan, S. J. (1992) *Plasmid 27*, 119−129.
17. Paulsen, I. T., Littlejohn, T. G., Radstrom, P., Sundstrom, L., Skold, O., Swedberg, G., and Skurray, R. A. (1993) *Antimicrob. Agents Chemother. 37*, 761−768.
18. Schuldiner, S., Granot, D., Steiner, S., Ninio, S., Rotem, D., Soskin, M., and Yerushalmi, H. (2001) *J. Mol. Microbiol. Biotechnol. 3*, 155−162.
19. Yerushalmi, H., Lebendiker, M., and Schuldiner, S. (1996) *J. Biol. Chem. 271*, 31044−31048.
20. de Groot, H. J. (2000) *Curr. Opin. Struct. Biol. 10*, 593−600.
21. Marassi, F. M., and Opella, S. J. (1998) *Curr. Opin. Struct. Biol. 8*, 640−648.
22. Kuhlbrandt, W., and Williams, K. A. (1999) *Curr. Opin. Chem. Biol. 3*, 537−543.
23. Saibil, H. R. (2000) *Nat. Struct. Biol. 7*, 711−714.
24. Bogusz, S., Boxer, A., and Busath, D. D. (1992) *Protein Eng. 5*, 285−293.
25. Durell, S. R., and Guy, H. R. (1992) *Biophys. J. 62*, 238−247.
26. Guy, H. R., and Seetharamulu, P. (1986) *Proc. Natl. Acad. Sci. U.S.A. 83*, 508−512.
27. Kerr, I. D., and Sansom, M. S. (1997) *Biophys. J. 73*, 581−602.
28. Ortells, M. O., and Lunt, G. G. (1996) *Protein Eng. 9*, 51−59.
29. Sato, C., and Matsumoto, G. (1995) *J. Membr. Biol. 147*, 45−70.
30. Jones, P. M. A., and George, A. M. (2000) *Eur. J. Biochem. 267*, 5298−5305.
31. Jones, P. M., and George, A. M. (1998) *J. Membr. Biol. 166*, 133−147.
32. Tsigelny, I., Sugiyama, N., Sine, S. M., and Taylor, P. (1997) *Biophys. J. 73*, 52−66.
33. Corbin, J., Methot, N., Wang, H. H., Baenziger, J. E., and Blanton, M. P. (1998) *J. Biol. Chem. 273*, 771−777.
34. Doak, D. G., Mulvey, D., Kawaguchi, K., Villalain, J., and Campbell, I. D. (1996) *J. Mol. Biol. 258*, 672−687.
35. Haris, P. I. (1998) *Biosci. Rep. 18*, 299−312.
36. Hunt, J. F., Earnest, T. N., Bousche, O., Kalghatgi, K., Reilly, K., Horvath, C., Rothschild, K. J., and Engelman, D. M. (1997) *Biochemistry 36*, 15156−15176.
37. Katragadda, M., Chopra, A., Bennett, M., Alderfer, J. L., Yeagle, P. L., and Albert, A. D. (2001) *J. Pept. Res. 58*, 79−89.
38. Wigley, W. C., Vijayakumar, S., Jones, J. D., Slaughter, C., and Thomas, P. J. (1998) *Biochemistry 37*, 844−853.
39. Xie, H., Ding, F. X., Schreiber, D., Eng, G., Liu, S. F., Arshava, B., Arevalo, E., Becker, J. M., and Naider, F. (2000) *Biochemistry 39*, 15462−15474.
40. Zhang, J. T., Chen, M., Han, E., and Wang, C. (1998) *Mol. Biol. Cell 9*, 853−863.
41. Aggeli, A., Bannister, M. L., Bell, M., Boden, N., Findlay, J. B., Hunter, M., Knowles, P. F., and Yang, J. C. (1998) *Biochemistry 37*, 8121−8131.
42. Ben-Efraim, I., Strahilevitz, J., Bach. D., and Shai, Y. (1994) *Biochemistry 33*, 6966−6973.
43. Ben-Efraim, I., and Shai, Y. (1996) *Protein Sci. 5*, 2287−2297.
44. Luneberg, J., Widmann, M., Dathe, M., and Marti, T. (1998) *J. Biol. Chem. 273*, 28822−28830.
45. Tatulian, S. A., and Tamm, L. K. (2000) *Biochemistry 39*, 496−507.
46. Horvath, L. I., Heimburg, T., Kovachev, P., Findlay, J. B., Hideg, K., and Marsh, D. (1995) *Biochemistry 34*, 3893−3898.
47. Ben-Efraim, I., and Shai, Y. (1997) *Biophys. J. 72*, 85−96.
48. Mercer, E. A., Abbott, G. W., Brazier, S. P., Ramesh, B., Haris, P. I., and Srai, S. K. (1997) *Biochem. J. 325*, 475−479.
49. Schuldiner, S., Lebendiker, M., and Yerushalmi, H. (1997) *J. Exp. Biol. 200*, 335−341.
50. Arkin, I. T., Russ, W. P., Lebendiker, M., and Schuldiner, S. (1996) *Biochemistry 35*, 7233−7238.
51. Schwaiger, M., Lebendiker, M., Yerushalmi, H., Coles, M., Groger, A., Schwarz, C., Schuldiner, S., and Kessler, H. (1998) *Eur. J. Biochem. 254*, 610−619.

52. Harroun, T. A., Heller, W. T., Weiss, T. M., Yang, L., and Huang, H. W. (1999) *Biophys. J. 76*, 3176−3185.
53. Killian, J. A. (1998) *Biochim. Biophys. Acta 1376*, 401−415.
54. Tate, C. G., Kunji, E. R., Lebendiker, M., and Schuldiner, S. (2001) *EMBO J. 20*, 77−81.
55. Balaram, P. (1999) *J. Pept. Res. 54*, 195−199.
56. Gellman, S. H. (1998) *Curr. Opin. Chem. Biol. 2*, 717−725.
57. Braunschweiler, L., and Ernst, R. R. (1983) *J. Magn. Reson. 53*, 521−528.
58. Kumar, A., Ernst, R. R., and Wuthrich, K. (1980) *Biochem. Biophys. Res. Commun. 95*, 1−6.
59. Piantini, U., Sorensen, O. W., and Ernst, R. R. (1982) *J. Am. Chem. Soc. 104*, 6800−6801.
60. Güntert, P., Mumenthaler, C., and Wüthrich, K. (1997) *J. Mol. Biol. 273*, 283−298.
61. Koradi, R., Billeter, M., and Wüthrich, K. (1996) *J. Mol. Graphics Modell. 14*, 51−55.
62. Helenius, A., McCaslin, D. R., Fries, E., and Tanford, C. (1979) *Methods Enzymol. 56*, 734−749.
63. Woody, R. W. (1995) *Methods Enzymol. 246*, 34−71.
64. Gunasekaran, K., Nagarajaram, H. A., Ramakrishnan, C., and Balaram, P. (1998) *J. Mol. Biol. 275*, 917−932.
65. Ulmschneider, M. B., and Sansom, M. S. (2001) *Biochim. Biophys. Acta 1512*, 1−14.
66. Damberg, P., Jarvet, J., and Graslund, A. (2001) *Methods Enzymol. 339*, 271−285.
67. Opella, S. J., Ma, C., and Marassi, F. M. (2001) *Methods Enzymol. 339*, 285−313.
68. Yerushalmi, H., and Schuldiner, S. (2000) *J. Biol. Chem. 275*, 5264−5269.
69. Wu, C. S., Hachimori, A., and Yang, J. T. (1982) *Biochemistry 21*, 4556−4562.
70. Oblatt-Montal, M., Buhler, L. K., Iwamoto, T., Tomich, J. M., and Montal, M. (1993) *J. Biol. Chem. 268*, 14601−14607.
71. Oblatt-Montal, M., Yamazaki, M., Nelson, R., and Montal, M. (1995) *Protein Sci. 4*, 1490−1497.
72. Reddy, G. L., Iwamoto, T., Tomich, J. M., and Montal, M. (1993) *J. Biol. Chem. 268*, 14608−14615.

BI015793W